Journal of Magnetic Resonance 350 (2023) 107423

Contents lists available at ScienceDirect

Journal of Magnetic Resonance

journal homepage: www.elsevier.com/locate/jmr

Pushing the limit of MQMAS for low-γ quadrupolar nuclei in pharmaceutical hydrochlorides

Ivan Hung, Zhehong Gan *

National High Magnetic Field Laboratory, 1800 East Paul Dirac Drive, Tallahassee, FL 32310, USA

ARTICLE INFO

Article history:
Received 3 February 2023
Revised 8 March 2023
Accepted 8 March 2023
Available online 12 March 2023

Keywords:
Multiple quantum magic-angle spinning
MQMAS
Active pharmaceutical ingredients
API
^{35}Cl
Hydrochloride
HCl
High magnetic field
Frequency crossing
Anti-crossing
Cosine pulse
Double-frequency
Magic-angle spinning
Spinning sidebands
Shearing

ABSTRACT

Solid-state NMR of quadrupolar nuclei such as ^{35}Cl has become a useful tool to characterize polymorphism in pharmaceutical hydrochlorides. The two-dimensional multiple-quantum magic-angle spinning (MQMAS) experiment can achieve isotropic resolution, and separate quadrupolar line shapes for samples with multiple sites but the pulse sequence efficiency is often low, limiting applications due to the intrinsically low NMR signals and *rf* field from the low gyromagnetic ratios γ. The use of cosine low-power MQMAS pulse sequences and high magnetic fields is presented to push the limit of MQMAS for insensitive low-γ quadrupolar nuclei. The improved efficiency and fields up to 35.2 T enable the acquisition of MQMAS spectra for pharmaceutical samples with multiple ^{35}Cl sites, large quadrupolar couplings and/or in diluted dosage forms.

1. Introduction

More than 50% of all available medicines exist in the form of solids as salts and hydrates. Active pharmaceutical ingredient (API) molecules can form distinct structural arrangements with hydrates and solvates known as polymorphs. Polymorphism is an important variable for adjusting physicochemical properties of APIs such as stability, solubility, density that are relevant to shelf life, dissolution, absorption, and effectiveness of drugs [1–3]. Solid-state NMR spectroscopy is a powerful tool for identifying and quantifying different polymorphs and solid forms of APIs [4–8]. ^{1}H, ^{19}F, ^{31}P, ^{13}C and ^{15}N NMR are usually used with their favorable spectral sensitivity and resolution considerations. The high spectral resolution of these spin S = 1/2 nuclei obtained under magic-angle spinning (MAS) enable the detection of small chemical shift changes induced by the structural differences of API molecules among polymorphs and formulations [9,10]. Most of the salt nuclei themselves are spin S > 1/2 quadrupolar nuclei like ^{35}Cl, ^{23}Na, ^{39}K and ^{43}Ca, and can also be sensitive targets for NMR study. For quadrupolar nuclei, their surrounding electric-field-gradient (EFG) can be measured in addition to the chemical shielding; both are sensitive to the spatial arrangements and interactions with surrounding API molecules such as electrostatic and hydrogen-bonding. In combination with X-ray diffraction and plane-wave density functional theory (DFT) calculations, solid-state NMR of quadrupolar nuclei has emerged as a complimentary tool to the investigation of spins S = 1/2 nuclei for structural characterization of APIs and polymorphism. Among these nuclei, ^{35}Cl stands out since HCl is the most used salt (15.5%) for drugs [11–22].

For half-integer spins, the second-order quadrupolar broadening and chemical shielding anisotropy (CSA) give rise to broad powder pattern line shapes. For samples with a single quadrupolar site, fitting of the static powder spectral line shape can be carried out to obtain the EFG and CSA tensor parameters. In the case of moderate quadrupolar broadening, magic-angle spinning (MAS) becomes useful as it averages out the CSA. The second-order quadrupolar interaction partially remains under MAS and can be

* Corresponding author.
E-mail address: gan@magnet.fsu.edu (Z. Gan).

https://doi.org/10.1016/j.jmr.2023.107423
1090-7807/

used to determine the quadrupolar coupling constant C_Q and EFG asymmetry parameter η_Q. For samples with multiple sites, the quadrupolar broadening poses challenges in both spectral resolution and sensitivity especially to nuclei with low gyromagnetic ratios γ. The CSA and second-order quadrupolar interactions have opposite field dependences, therefore the availability of high magnetic fields is of great help to narrow the quadrupolar broadening and to untangle multi-parameter fitting of the EFG and CSA interactions. Furthermore, two-dimensional (2D) methods such as multiple-quantum magic-angle spinning (MQMAS) [23] are the ultimate tool for obtaining isotropic spectra and separating quadrupolar powder patterns into two dimensions. Applications of the powerful MQMAS method are often limited by the low experimental efficiency especially for low-γ quadrupolar nuclei. The efficiency of generating multiple-quantum (MQ) coherence followed by conversion to central-transition (CT) coherence for signal detection depends strongly on the *rf* field strength $\omega_1 = \gamma B_1$ relative to the quadrupolar coupling [24,25]. The efficiency can become prohibitively low for low-γ quadrupolar nuclei due to their intrinsically low γB_1 on top of their inherently weak NMR signals and large quadrupolar broadening. Various phase-modulated methods [26–29] and the satellite transition magic-angle spinning (STMAS) variant [30] have been developed to address this issue for MQMAS applications. Recently, a novel approach using rotor-period long pulses to selectively irradiate the satellite-transitions (STs) was introduced. The new method utilizes the frequency crossings of the *rf* pulses induced by MAS with the STs in a coherent and efficient manner [31,32], and has succeeded in the acquisition of MQMAS and STMAS spectra for the largest quadrupolar coupling to date [33–35]. A key feature of the long-pulse method is its low *rf* power requirement as compared to the traditional short-pulse methods. In this contribution, we apply the latest cosine low-power MQMAS (cos-lpMQMAS) pulse sequence [35] with ultrahigh magnetic fields up to 35.2 T available at the National High Magnetic Field Laboratory (NHMFL) [36]. The low power requirement, and gains in spectral sensitivity and resolution from high magnetic fields push the limit of MQMAS for low-γ quadrupolar nuclei for challenging API samples with multiple ^{35}Cl sites, large quadrupolar couplings, and/or in diluted dosage form.

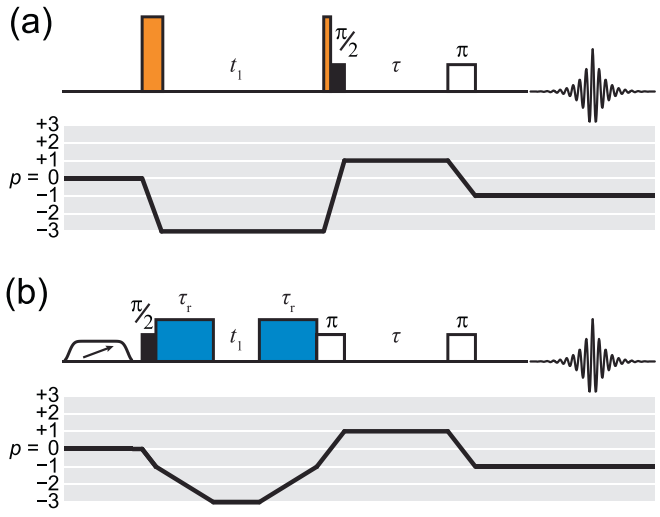

Fig. 1. Pulse sequence schematics for the (a) short-pulse MQMAS [29] and (b) cos-lpMQMAS [35] pulse sequences.

2. Results and discussion

Fig. 1 shows the short-pulse MQMAS and cos-lpMQMAS pulse sequences. The key element of cos-lpMQMAS are the rotor-period long pulses (Fig. 1b, blue) with cosine amplitude modulation, which splits the irradiation from the central-transition (CT) to the satellite-transitions (STs). The cosine modulation is similar to the double-frequency sweep (DFS) but without the sweeping part [27,37]. The modulation frequency applied is within the span of the STs but far enough away from the CT to make it selective only to the STs. The goal of this cosine pulse for the MQMAS experiment is to selectively invert the $|\pm3/2> \leftrightarrow |\pm1/2>$ spin states. Ideally, a ST-selective π-pulse would fully interconvert the CT and triple-quantum (3Q) coherences [34,38]. For a rotor-period long pulse, the ST frequencies are modulated by the MAS and sweep across the *rf* frequency. These *rf* crossings are effective for the $|\pm3/2> \leftrightarrow |\pm1/2>$ transitions, but the timing and sweep rate of the passages vary widely among the crystallites in a powder sample. It has been shown that the average *rf* Hamiltonian can be described by a scaled effective *rf* field with a phase shift equal to the ST spinning sidebands near the *rf* frequency [31,32]. It is important to note that the phase of spinning sidebands distributes widely among individual crystallites, and it becomes absorptive only after averaging over the rotor phase angle. The phase distribution of the effective *rf* field usually causes signal cancellation for powder samples, however, it can be avoided by designing the MQMAS pulse in a symmetric manner using two identical rotor-period long pulses with opposite changes of coherence orders for the multiple-quantum excitation and conversion as shown in Fig. 1b. One can use the frequency encoding block with two $\pi/2$-pulses commonly used for the indirect dimension of 2D experiments to understand this. The encoding of either the cosine or sine amplitude modulation is determined only by the relative phase of the two pulses. Their absolute phase or its phase distribution here does not matter, therefore it does not lead to signal cancellation for the 2D experiment. This is the main idea of MQMAS pulse sequences using rotor-period long ST pulses, either for the amplitude-modulated z-filtered or phase-modulated shifted-echo version. It is worth mentioning that this method works particularly well for large quadrupolar couplings and for spin $S = 3/2$ nuclei which have a single pair of STs. The confinement within a two-level ST system helps to constrain the coherence transfer to the desired CT $\leftrightarrow$ 3Q transfer. A more detailed description and theory about the long-pulse and frequency-crossing mechanism can be found in Refs. [31–33,35].

A sample of K_2SO_4 is first used to demonstrate and compare the MQMAS pulse sequences for the spin $S = 3/2$ low-γ quadrupolar nucleus ^{39}K. Fig. 2a shows a 21% efficiency for the conventional short-pulse method using the maximum attainable *rf* field of $\nu_1 \sim 70$ kHz (at ~ 800 W) for the 3.2 mm MAS probe that was used. A CT-selective $\pi/2$ pulse (black in Fig. 1a) was used to enhance the MQ $\rightarrow$ CT conversion [29]. The efficiency for cos-lpMQMAS is 38%, almost two folds compared to using short pulses but with significantly lower *rf* power of 300 W corresponding to a *rf* field of $\nu_1 \sim 43$ kHz. The K_2SO_4 sample was chosen for calibration and comparison of the MQMAS pulse sequences since its relatively small ^{39}K C_Q and good signals make MQMAS relatively easy to acquire. Numerical simulations have shown that the MQMAS efficiency drops dramatically with the ratio of C_Q/ν_1 [24,33]. The gain by cos-lpMQMAS becomes much more for samples with larger C_Q. The ν_1 calibration curve in Fig. 2c shows the efficiency starting to level off at $\nu_1 \sim 36$ kHz. The low ν_1 requirement and its ability to acquire spectra with large C_Q makes cos-lpMQMAS particularly suitable for low-γ nuclei with large quadrupolar broadening as well as challenging API samples with intrinsically weak NMR sig-

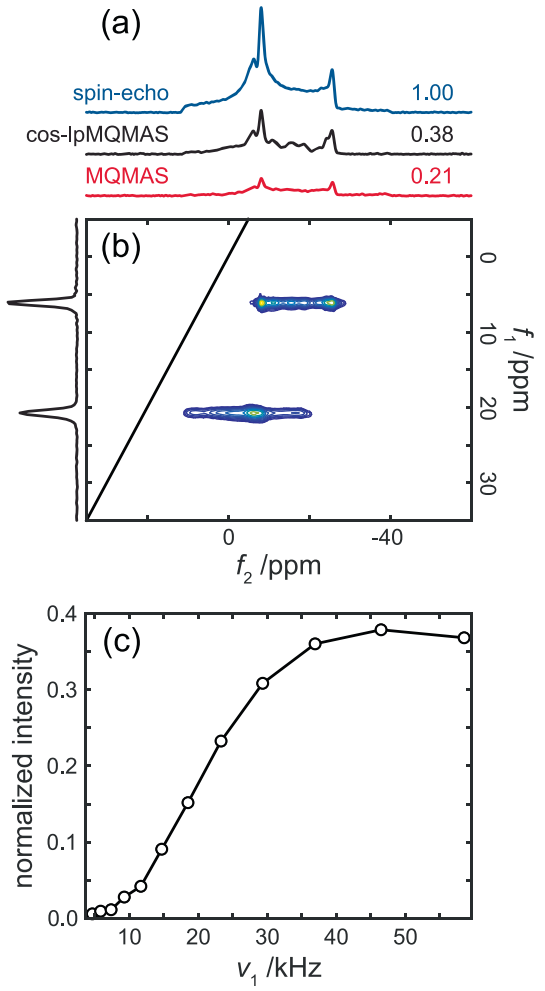

Fig. 2. (a) Comparison of efficiencies with the first t_1 increments of the short-pulse MQMAS and cos-lpMQMAS experiments. The numerical efficiencies are obtained from the integrated intensity compared to a spin-echo spectrum acquired using the same number of scans and recycle delays. (b) 2D ^{39}K MQMAS spectrum of K_2SO_4 with isotropic projection to the left. (c) Normalized intensity for the first t_1-point of the cos-lpMQMAS experiment as a function of the ^{39}K *rf* field $\gamma B_1/2\pi$ applied for the rotor-period long CT ↔ 3Q pulses. Experiments were carried out at B_0 = 19.6 T at a frequency of $\nu_0(^{39}K)$ = 38.8 MHz using a Bruker Avance NEO spectrometer and a Low-E 3.2 mm MAS probe developed at the NHMFL. A spinning frequency of $\omega_r/2\pi$ = 16 kHz was used, and where applicable, 'soft' π/2- and π-pulses of 20 and 40 μs with *rf* fields of 6.25 kHz. Pulses of 10.8 and 3.6 μs with $\nu_1 \sim 70$ kHz were used for 3Q excitation and conversion in the short-pulse MQMAS experiment. For cos-lpMQMAS, rotor-period long pulses were used with $\nu_1 \sim 43$ kHz and an amplitude modulation corresponding to a transmitter offset of ± 192 kHz, and signal enhancement using a 1.5 ms WURST-80 pulse with a sweep range equal to ν_r, $\nu_1 \sim 19$ kHz, and offset of +250 kHz. For each spectrum in (a), 96 transients were averaged with a recycle delay of 20 s; in (b), 96 transients were averaged for each of the 128 complex t_1 points using a 2 s recycle delay, resulting in an experimental time of ~7 h.

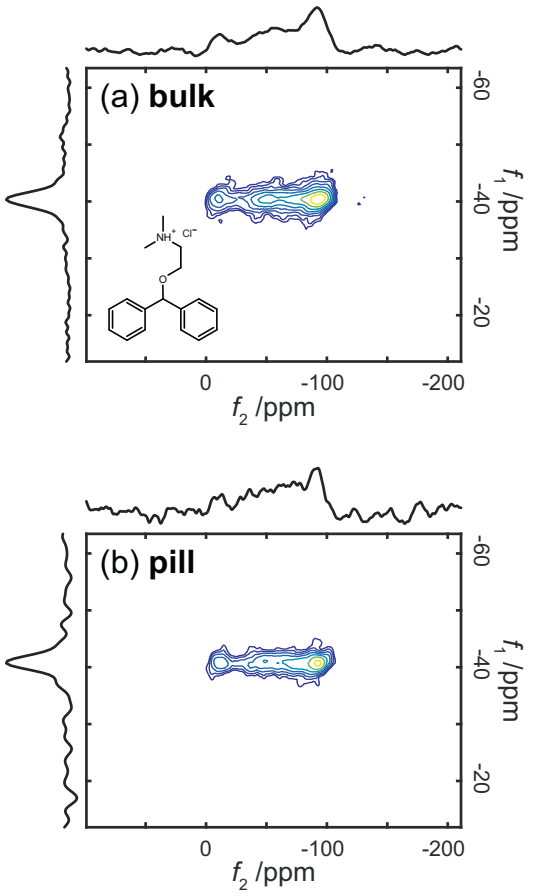

Fig. 3. 2D ^{35}Cl cos-lpMQMAS NMR spectra of diphenhydramine·HCl in (a) pure bulk polycrystalline and (b) diluted dosage pill forms. Experiments were carried out at B_0 = 19.6 T at a frequency of $\nu_0(^{35}Cl)$ = 81.4 MHz using a Bruker Avance NEO spectrometer and a Low-E 3.2 mm MAS probe developed at the NHMFL. A spinning frequency of $\omega_r/2\pi$ = 16 kHz was used, and 'soft' π/2- and π-pulses of 4 and 8 μs with *rf* fields of 31.25 kHz. Rotor-period long pulses were used for CT ↔ 3Q interconversion with $\nu_1 \sim 69$ kHz and an amplitude modulation corresponding to a transmitter offset of ± 256 kHz. Signal enhancement was performed using a 2 ms WURST-80 pulse with a sweep range equal to ν_r, $\nu_1 \sim 13$ kHz, and offset of +256 kHz. For (a), 4800 transients were averaged for each of the 32 complex t_1 points using a 25 ms recycle delay, resulting in an experimental time of ~ 64 min. For (b), 108,000 transients were averaged for each of the 16 complex t_1 points using a 25 ms recycle delay, resulting in an experimental time of ~720 min.

nals. It is also worth further mention that a strong C_Q/ν_1 dependence affects MQMAS spectral quantitation which is often important to pharmaceutical applications. The cos-lpMQMAS helps to reduce but does not fully negate this dependence for more quantitative analysis.

Fig. 3 shows that ^{35}Cl MQMAS spectra can be acquired for APIs such as diphenhydramine·HCl in pure polycrystalline form as well as in the Benadryl® diluted dosage form within 1.1 and 12 h, respectively, at 19.6 T. A comparison between the two spectra shows no difference along the isotropic and acquisition dimensions, an indication that the ^{35}Cl EFG and API molecules remain intact as in their pure crystalline form and are not affected by addition of excipients during preparation of the dosage form, as has been reported [20]. Remarkably, the high magnetic field and enhanced efficiency from using cos-lpMQMAS enable acquisition of an isotropic ^{35}Cl spectrum for ~30 mg of a crushed Benadryl® pill, which contains only ~6% by weight of the diphenhydramine·HCl API.

The high isotropic resolution from MQMAS is particularly powerful for separating overlapped powder patterns in two dimensions as demonstrated in Fig. 4 for a previously studied polymorph of Isoxsuprine·HCl (Isox-II) [18,20,39]. Isox-II has two inequivalent ^{35}Cl sites with large quadrupolar couplings which cause (1) complete overlap due to the second-order quadrupolar broadening, and (2) unresolved spinning sidebands (ssbs) with the 16 kHz MAS frequency used even at a high magnetic field of 19.6 T. The overlap makes deconvolution and fitting of the spectral line shapes difficult. The powder patterns and their ssbs become separated in the 2D MQMAS spectra. For large quadrupolar couplings, it is worth discussing the ssbs in 2D MQMAS spectra considering the limited spinning speed of larger diameter rotors typically used for detecting weak NMR signals of low-γ quadrupolar nuclei due

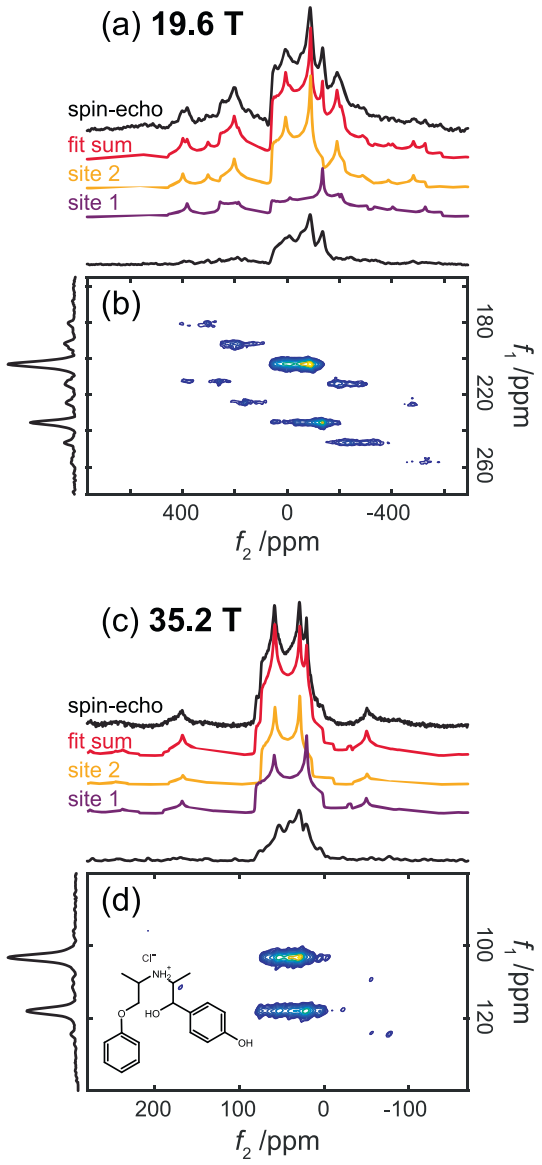

Fig. 4. ^{35}Cl 1D spin-echo and 2D cos-lpMQMAS NMR spectra of pure polycrystalline isoxsuprine·HCl acquired at (a,b) 19.6 ($\nu_0(^{35}Cl)$ = 81.4 MHz), and (c,d) 35.2 T (ν_0-(^{35}Cl) = 147.0 MHz). Fitting of the two ^{35}Cl sites performed using SOLA within the Bruker Topspin 4.1.1 software package are shown in (a) and (c). Experiments were carried out using Bruker Avance NEO spectrometers and 3.2 mm MAS probes developed at the NHMFL. A spinning frequency of $\omega_r/2\pi$ = 16 kHz was used in both cases. For (b), 'soft' π/2- and π-pulses of 4 and 8 μs with *rf* fields of 31.25 kHz were used along with rotor-period long pulses for CT ↔ 3Q interconversion with ν_1- ~ 78 kHz and an amplitude modulation corresponding to a transmitter offset of ± 320 kHz; 36,000 transients were averaged for each of the 26 complex t_1 points using a 150 ms recycle delay, resulting in an experimental time of ~39 h. Signal enhancement was performed using a 2 ms WURST-80 pulse with a sweep range equal to ν_r, ν_1 ~ 20 kHz, and offset of + 320 kHz. For (d), 'soft' π/2- and π-pulses of 5 and 10 μs with *rf* fields of 25 kHz were used along with rotor-period long pulses for CT ↔ 3Q interconversion with ν_1 ~ 73 kHz and an amplitude modulation corresponding to a transmitter offset of ±320 kHz; 2400 transients were averaged for each of the 16 complex t_1 points using a 200 ms recycle delay, resulting in an experimental time of ~2.1 h.

to their large sample volumes. For the MQMAS experiment, the MQ excitation and conversion efficiencies are rotor-angle dependent, therefore they can contribute rotor modulation [40] in addition to the anisotropic MQ frequency modulation when t_1 evolution is not rotor-synchronized. The CSA portion of the latter is three-fold larger for the 3Q transition. All spectra presented in this work were acquired with rotor-synchronized t_1 evolution to avoid any rotor modulations and ssbs along the indirect MQ dimension. Rotor-synchronization restricts the F_1 spectral window to the spinning frequency, which can lead to peak folding including the CT ssbs that remain along the F_2 dimension as shown in Fig. 4. The *Q*-shear method [41] can unfold aliasing of the ssbs by expanding the F_1 window via zero-filling. The key step of the procedure is a shear by an integer slope k_Q prior to F_1 zero-filling followed by isotropic shearing at k_{iso}. A k_Q = −3 shear would eliminate the chemical shift and folding along the 3Q F_1 dimension [41]. For the spin S = 3/2 ^{35}Cl nuclei in Fig. 4, the dominant broadening is the second-order quadrupolar broadening along the 3Q F_1 dimension which has a slope k_{iso} = −7/9 with respect to the CT. In this instance, the 2D spectra were first sheared by a slope of k_Q = −1. This first shear does not eliminate chemical shift completely but reduces the quadrupolar broadening and keeps the ssbs aligned in F_1 within the spectral window which is equal to the spinning frequency. Then the 2D spectra were zero-filled in both directions to obtain an enlarged F_1 spectral window such that the carrier frequency remains centered. A second shear was applied by a slope of (k_Q - k_{iso}) to obtain the final isotropically sheared MQMAS spectra. For spin S = 3/2 nuclei, the ssbs appear at a slope of k_{iso} = −7/9 in frequency units after isotropic shearing, an opposite sign slope results for spins S > 3/2. Fig. 4a shows that using this shearing procedure the ssbs become untangled in an ordered manner along F_1. It is important to note that the ssbs originate from the anisotropic CT frequency modulated by MAS in F_2, and therefore can be fitted accordingly if needed despite appearing in both dimensions after the spectral shearing [42]. At 19.6 T, there are at least 5 ssbs visible in Fig. 4a. The spread of signal intensity among the ssbs lowers the peak height affecting the signal-to-noise ratio and needs to be considered when performing quantitative analysis.

Higher magnet fields help to simplify the MQMAS spectra of samples where the second-order quadrupolar interaction dominates over the CSA, as is common for API hydrochlorides. Fig. 4b shows that the ssbs mostly disappear in the MQMAS spectrum of Isox-II acquired at 35.2 T using the same spinning frequency in ~2.1 h; almost a factor 20 less in time. Besides the known sensitivity gains from polarization, resonance frequency and line narrowing, the concentration of signal intensities from the ssbs to the center-band at the higher field provides an additional sensitivity gain, contributing to the dramatic time savings.

MQMAS spectra at different fields help to separate the isotropic chemical shift δ_{iso} and second-order quadrupolar shift δ_{QIS} due to their different field dependences in frequency units. The isotropic peak position along F_1 and the mass center position in F_2 are given by

$$\delta_1 = \delta_{iso} - (10/17)\delta_{QIS}, \quad \delta_2 = \delta_{iso} + \delta_{QIS} \tag{1}$$

$$\delta_{QIS} = \frac{P_Q^2}{\nu_0^2} \cdot \frac{3\left[\frac{3}{4} - S(S+1)\right]}{10[2S(2S-1)]^2} \cdot 10^6$$

The MQMAS efficiency including for cos-lpMQMAS has orientational variations that can distort the line shape, affecting the fitting of the line shape extracted directly from the 2D spectra. Nevertheless, the F_1 peak position and the mass center along F_2 provide constraints on the chemical shift and isotropic shifts given in Eq. (1), which helps to deconvolute spectral features observed in 1D spectra. The isotropic resolution can also reveal the presence of minor components and/or disorder. Fig. 4 shows fits of the 1D spin-echo spectra with the following parameters obtained for Isox-II: δ_{iso} = 90-ppm, C_Q = 6.4 MHz, η_Q = 0.33; δ_{iso} = 81 ppm, C_Q = 5.6 MHz, η_Q = 0.32 in good agreement with a previous study [20]; noting that the reported isotropic chemical shifts were referenced to solid NaCl (−41.1 ppm) vs. the 0.1 M NaCl D_2O solution (0 ppm) used in this work [43].

3. Conclusions

It has been shown that the cos-lpMQMAS experiment utilizes the mechanism of frequency crossings with satellite-transitions to excite and convert MQ transitions efficiently. The excitation and conversion segments are designed such that the two work together coherently to avoid signal cancellation. The long-pulse scheme has two key features. First, it lowers the *rf* field requirement, making cos-lpMQMAS suitable for low-γ quadrupolar nuclei such as ^{35}Cl in pharmaceutical hydrochloride samples. Second, the MQMAS efficiency with the long-pulse scheme decreases much slower with increase in the quadrupolar coupling than for conventional short-pulse MQMAS sequences, enabling its application to challenging API samples with large quadrupolar couplings for resolution of spectral overlap among multiple sites even in diluted dosage forms. Furthermore, a comparison between 19.6 and 35.2 T has demonstrated dramatic gains in overall spectral sensitivity by high magnetic fields. The combination of efficient pulse sequences and high magnetic fields extends the limit of application for the MQMAS method, and its power to resolve spectral overlap in two dimensions.

Data availability

Data will be made available on request.

Declaration of Competing Interest

The authors declare that they have no known competing financial interests or personal relationships that could have appeared to influence the work reported in this paper.

Acknowledgements

This work was supported by the National High Magnetic Field Laboratory (NHMFL, USA) through NSF DMR-1644779 and the State of Florida. Development of the 36T SCH magnet and NMR instrumentation was supported by NSF (DMR-1039938 and DMR-0603042) and NIH (BTRR 1P41 GM122698). API samples were kindly provided by the group of Prof. Robert W. Schurko.

References

[1] J.K. Haleblian, Characterization of Habits and Crystalline Modification of Solids and Their Pharmaceutical Applications, J. Pharm. Sci. 64 (1975) 1269–1288, https://doi.org/10.1002/jps.2600640805.
[2] L.-F. Huang, W.-Q. Tong, Impact of solid state properties on developability assessment of drug candidates, Adv. Drug Deliv. Rev. 56 (2004) 321–334, https://doi.org/10.1016/j.addr.2003.10.007.
[3] D. Singhal, W. Curatolo, Drug polymorphism and dosage form design: a practical perspective, Adv. Drug Deliv. Rev. 56 (2004) 335–347, https://doi.org/10.1016/j.addr.2003.10.008.
[4] A. Watts, Solid-state NMR in drug design and discovery for membrane-embedded targets, Nat. Rev. Drug Discov. 4 (2005) 555–568, https://doi.org/10.1038/nrd1773.
[5] R.T. Berendt, D.M. Sperger, P.K. Isbester, E.J. Munson, Solid-state NMR spectroscopy in pharmaceutical research and analysis, Trends Anal. Chem. 25 (2006) 977–984, https://doi.org/10.1016/j.trac.2006.07.006.
[6] R.K. Harris, Applications of solid-state NMR to pharmaceutical polymorphism and related matters, J. Pharm. Pharmacol. 59 (2007) 225–239, https://doi.org/10.1211/jpp.59.2.0009.
[7] M. Geppi, G. Mollica, S. Borsacchi, C.A. Veracini, Solid-state NMR studies of pharmaceutical systems, Appl. Spectrosc. Rev. 43 (2008) 202–302, https://doi.org/10.1080/05704920801944338.
[8] F.G. Vogt, Characterization of Pharmaceutical Compounds by Solid-state NMR, in: EMagRes, John Wiley & Sons, Ltd, 2015, pp. 255–268. 10.1002/9780470034590.emrstm1393.
[9] M. Li, W. Xu, Y. Su, Solid-state NMR spectroscopy in pharmaceutical sciences, Trends Anal. Chem. 135 (2021), https://doi.org/10.1016/j.trac.2020.116152.
[10] Y. Du, Y. Su, 19F Solid-state NMR characterization of pharmaceutical solids, Solid State Nucl. Magn. Reson. 120 (2022), https://doi.org/10.1016/j.ssnmr.2022.101796.
[11] D.L. Bryce, G.D. Sward, S. Adiga, Solid-state 35/37Cl NMR spectroscopy of hydrochloride salts of amino acids implicated in chloride ion transport channel selectivity: Opportunities at 900 MHz, J. Am. Chem. Soc. 128 (2006) 2121–2134.
[12] R.P. Chapman, D.L. Bryce, A high-field solid-state Cl-35/37 NMR and quantum chemical investigation of the chlorine quadrupolar and chemical shift tensors in amino acid hydrochlorides, Phys. Chem. Chem. Phys. 9 (2007) 6219–6230.
[13] H. Hamaed, J.M. Pawlowski, B.F.T. Cooper, R.Q. Fu, S.H. Eichhorn, R.W. Schurko, Application of solid-state Cl-35 NMR to the structural characterization of hydrochloride pharmaceuticals and their polymorphs, J. Am. Chem. Soc. 130 (2008) 11056–11065.
[14] R.P. Chapman, J.R. Hiscock, P.A. Gale, D.L. Bryce, A solid-state Cl-35/37 NMR study of a chloride ion receptor and a GIPAW-DFT study of chlorine NMR interaction tensors in organic hydrochlorides, Can. J. Chem.-Rev. Can. Chim. 89 (2011) 822–834, https://doi.org/10.1139/V10-177.
[15] R.J. Attrell, C.M. Widdifield, I. Korobkov, D.L. Bryce, Weak Halogen Bonding in Solid Haloanilinium Halides Probed Directly via Chlorine-35, Bromine-81, and Iodine-127 NMR Spectroscopy, Cryst. Growth Des. 12 (2012) 1641–1653, https://doi.org/10.1021/cg201683p.
[16] F.G. Vogt, G.R. Williams, M.N. Johnson, R.C.B. Copley, A Spectroscopic and Diffractometric Study of Polymorphism in Ethyl 3-{3-[((2R)-3-{[2-(2,3-dihydro-1H-inden-2-yl)-1,1-dimethylethyl]amino}-2-hydroxypropyl)oxy]-4,5-difluorophenyl}propanoate Hydrochloride, Cryst. Growth Des. 13 (2013) 5353–5367, https://doi.org/10.1021/cg401232g.
[17] F.G. Vogt, G.R. Williams, R.C.B. Copley, Solid-State NMR Analysis of a Boron-Containing Pharmaceutical Hydrochloride Salt, J. Pharm. Sci. 102 (2013) 3705–3716, https://doi.org/10.1002/jps.23679.
[18] M. Hildebrand, H. Hamaed, A.M. Namespetra, J.M. Donohue, R. Fu, I. Hung, Z. Gan, R.W. Schurko, 35Cl solid-state NMR of HCl salts of active pharmaceutical ingredients: structural prediction, spectral fingerprinting and polymorph recognition, CrystEngComm 16 (2014) 7334–7356, https://doi.org/10.1039/C4CE00544A.
[19] F.G. Vogt, G.R. Williams, M. Strohmeier, M.N. Johnson, R.C.B. Copley, Solid-State NMR Analysis of a Complex Crystalline Phase of Ronacaleret Hydrochloride, J. Phys. Chem. B 118 (2014) 10266–10284, https://doi.org/10.1021/jp505061j.
[20] A.M. Namespetra, D.A. Hirsh, M.P. Hildebrand, A.R. Sandre, H. Hamaed, J.M. Rawson, R.W. Schurko, 35Cl solid-state NMR spectroscopy of HCl pharmaceuticals and their polymorphs in bulk and dosage forms, CrystEngComm 18 (2016) 6213–6232, https://doi.org/10.1039/C6CE01069E.
[21] D.A. Hirsh, A.J. Rossini, L. Emsley, R.W. Schurko, Cl-35 dynamic nuclear polarization solid-state NMR of active pharmaceutical ingredients, Phys. Chem. Chem. Phys. 18 (2016) 25893–25904, https://doi.org/10.1039/c6cp04353d.
[22] D.A. Hirsh, Y. Su, H. Nie, W. Xu, D. Stueber, N. Variankaval, R.W. Schurko, Quantifying Disproportionation in Pharmaceutical Formulations with ^{35}Cl Solid-State NMR, Mol. Pharm. 15 (2018) 4038–4048, https://doi.org/10.1021/acs.molpharmaceut.8b00470.
[23] L. Frydman, J.S. Harwood, Isotropic Spectra of Half-Integer Quadrupolar Spins from Bidimensional Magic-Angle-Spinning NMR, J. Am. Chem. Soc. 117 (1995) 5367–5368.
[24] J.-P. Amoureux, C. Fernandez, L. Frydman, Optimized multiple-quantum magic-angle spinning NMR experiments on half-integer quadrupoles, Chem. Phys. Lett. 259 (1996) 347–355, https://doi.org/10.1016/0009-2614(96)00809-3.
[25] Z. Gan, P.L. Gor'kov, W.W. Brey, P.J. Sideris, C.P. Grey, Enhancing MQMAS of low-gamma nuclei by using a high B-1 field balanced probe circuit, J. Magn. Reson. 200 (2009) 2–5.
[26] G. Wu, D. Rovnyak, R.G. Griffin, Quantitative multiple-quantum magic-angle-spinning NMR spectroscopy of quadrupolar nuclei in solids, J. Am. Chem. Soc. 118 (1996) 9326–9332.
[27] A.P.M. Kentgens, R. Verhagen, Advantages of double frequency sweeps in static, MAS and MQMAS NMR of spin I=3/2 nuclei, Chem. Phys. Lett. 300 (1999) 435–443.
[28] P.K. Madhu, A. Goldbourt, L. Frydman, S. Vega, Sensitivity enhancement of the MQMAS NMR experiment by fast amplitude modulation of the pulses, Chem. Phys. Lett. 307 (1999) 41–47.
[29] Z.H. Gan, H.T. Kwak, Enhancing MQMAS sensitivity using signals from multiple coherence transfer pathways, J. Magn. Reson. 168 (2004) 346–351.
[30] Z. Gan, Isotropic NMR spectra of half-integer quadrupolar nuclei using satellite transitions and magic-angle spinning, J. Am. Chem. Soc. 122 (2000) 3242–3243.
[31] A.J. Pell, K.J. Sanders, S. Wegner, G. Pintacuda, C.P. Grey, Low-power broadband solid-state MAS NMR of 14N, J. Chem. Phys. 146 (2017).
[32] I. Hung, P. Gor'kov, Z. Gan, Efficient and sideband-free 1H-detected 14N magic-angle spinning NMR, J. Chem. Phys. 151 (2019), https://doi.org/10.1063/1.5126599.
[33] I. Hung, Z. Gan, Low-power STMAS – breaking through the limit of large quadrupolar interactions in high-resolution solid-state NMR spectroscopy, Phys. Chem. Chem. Phys. 22 (2020) 21119–21123, https://doi.org/10.1039/d0cp04274a.

[34] I. Hung, Isotropic solid-state MQMAS NMR spectra for large quadrupolar interactions using satellite-transition selective inversion pulses and low rf fields, J. Magn. Reson. 324 (2021), https://doi.org/10.1016/j.jmr.2021.106913.
[35] I. Hung, Z. Gan, On the use of single-frequency versus double-frequency satellite-transition pulses for MQMAS, J. Magn. Reson. 328 (2021), https://doi.org/10.1016/j.jmr.2021.106994.
[36] Z. Gan, I. Hung, X.L. Wang, J. Paulino, G. Wu, I.M. Litvak, P.L. Gor'kov, W.W. Brey, P. Lendi, J.L. Schiano, M.D. Bird, L.R. Dixon, J. Toth, G.S. Boebinger, T.A. Cross, NMR spectroscopy up to 35.2 T using a series-connected hybrid magnet, J. Magn. Reson. 284 (2017) 125–136, https://doi.org/10.1016/j.jmr.2017.08.007.
[37] D. Iuga, H. Schäfer, R. Verhagen, A.P.M. Kentgens, Population and Coherence Transfer Induced by Double Frequency Sweeps in Half-Integer Quadrupolar Spin Systems, J. Magn. Reson. 147 (2000) 192–209, https://doi.org/10.1006/jmre.2000.2192.
[38] H.T. Kwak, Z.H. Gan, Double-quantum filtered STMAS, J. Magn. Reson. 164 (2003) 369–372.
[39] I. Hung, Z. Gan, High Resolution NMR of S = 3/2 Quadrupole Nuclei by Detection of Double-Quantum Satellite-Transitions via Protons, J. Phys. Chem. Lett. 11 (2020) 4734–4740, https://doi.org/10.1021/acs.jpclett.0c01236.
[40] D. Massiot, Sensitivity and lineshape improvements of MQ-MAS by rotor-synchronized data acquisition, J. Magn. Reson. A 122 (1996) 240–244.
[41] I. Hung, J. Trebosc, G.L. Hoatson, R.L. Vold, J.P. Amoureux, Z. Gan, Q-shear transformation for MQMAS and STMAS NMR spectra, J. Magn. Reson. 201 (2009) 81–86.
[42] V. Martins, J. Xu, X. Wang, K. Chen, I. Hung, Z. Gan, C. Gervais, C. Bonhomme, S. Jiang, A. Zheng, B.E.G. Lucier, Y. Huang, Higher Magnetic Fields, Finer MOF Structural Information: O-17 Solid-State NMR at 35.2 T, J. Am. Chem. Soc. 142 (2020) 14877–14889, https://doi.org/10.1021/jacs.0c02810.
[43] R.P. Chapman, C.M. Widdifield, D.L. Bryce, Solid-state NMR of quadrupolar halogen nuclei, Prog. Nucl. Magn. Reson. Spectrosc. 55 (2009) 215–237, https://doi.org/10.1016/j.pnmrs.2009.05.001.